minerals

MDPI

Article

Experimental Etching of Diamonds: Extrapolation to Impact Diamonds from the Popigai Crater (Russia)

Valeri Sonin, Egor Zhimulev, Aleksei Chepurov *, Ivan Gryaznov, Anatoly Chepurov, Valentin Afanasiev and Nikolai Pokhilenko

V.S. Sobolev Institute of Geology and Mineralogy SB RAS, 3 Akademika Koptyuga, 630090 Novosibirsk, Russia; sonin@igm.nsc.ru (V.S.); ezhimulev@igm.nsc.ru (E.Z.); gryaznovia@igm.nsc.ru (I.G.); chepurov@igm.nsc.ru (A.C.); morpho@igm.nsc.ru (V.A.); chief@igm.nsc.ru (N.P.)
* Correspondence: achepurov@igm.nsc.ru

Abstract: Diamond etching in high-temperature ambient-pressure experiments has been performed aimed to assess possible postimpact effects on diamonds in impact craters, for the case of the Popigai crater in Yakutia (Russia). The experiments with different etchants, including various combinations of silicate melts, air, and inert gases, demonstrated the diversity of microstructures on {111} diamond faces: negative or positive trigons, as well as hexagonal, round, or irregularly shaped etch pits and striation. The surface features obtained after etching experiments with kimberlitic diamonds are similar to those observed on natural impact diamonds with some difference due to the origin of the latter as a result of a martensitic transformation of graphite in target rocks. Extrapolated to natural impact diamonds, the experimental results lead to several inferences: (1) Diamond crystals experienced natural oxidation and surface graphitization during the pressure decrease after the impact event, while the molten target rocks remained at high temperatures. (2) Natural etching of diamonds in silicate melts is possible in a large range of oxidation states controlled by O_2 diffusion. (3) Impact diamonds near the surface of molten target rocks oxidized at the highest rates, whereas those within the melt were shielded from the oxidizing agents and remained unchanged.

Keywords: impact diamonds; etching experiments; crystal morphology; oxidation; surface graphitization; Popigai impact crater

Citation: Sonin, V.; Zhimulev, E.; Chepurov, A.; Gryaznov, I.; Chepurov, A.; Afanasiev, V.; Pokhilenko, N. Experimental Etching of Diamonds: Extrapolation to Impact Diamonds from the Popigai Crater (Russia). *Minerals* **2021**, *11*, 1229. https://doi.org/10.3390/min11111229

Academic Editor: David Phillips

Received: 6 October 2021
Accepted: 1 November 2021
Published: 5 November 2021

1. Introduction

Natural diamonds form in the Earth's mantle at high pressures and temperatures, and they acquire different morphologies depending on their environment, rate of growth, etc. However, the morphology of diamond crystals can change in the postcrystallization history by dissolution (oxidation) under the effect of different agents, especially the melts that carry them to the surface. Dissolution of diamonds has been quite well studied in kimberlite melts [1–8], as well as in mantle Fe(+Ni)-S-C liquid [9–13], which may be their growth medium [14,15].

Diamonds found in impact craters, such as Kara, Ust'-Kara, and Puchezh-Katun in Russia; Bilylivka (Zapadnaya), Illintsi, Rotmistrivka, Bovtyshka, Zelenyi Gayi, Terny, and Obolon', as well as in some Neogene titanium-zirconium placers on the Ukrainian Shield; Ries in Germany; and Sudbury in Canada [16], have received much attention recently. The Popigai impact crater located in East Siberia, Russia [17–19], is of special interest in this respect. It stores plenty of extremely hard and stable impact diamonds exceeding the world resources of kimberlitic diamond [20,21].

The Popigai diamonds are pseudomorphs after graphite [19,22] resulting from an impact by a large bolide and shock metamorphism. The abundant crystalline graphite in the target rocks underwent martensitic transformation to a polycrystalline aggregate of nanometer cubic (diamond) and hexagonal (lonsdaleite) grains [23,24] with the predominant cubic phase [17,18,25]. The impact diamonds inherit the morphology of primary

graphite while decreasing in volume by a factor of 1.6, which is the graphite/diamond density difference.

The impact energy also caused melting of the target Archean gneisses, whereby diamond converted from graphite became exposed to hot silicate melt, with the ensuing partial graphitization and resorption. That is especially true for diamonds from tagamites which stayed for a long time in hot melt and underwent sintering, dissolution, and graphitization that resulted in the surface sculptures uncommon to primary graphite. The diamond content in tagamites is ~1.5 times greater than that in their high-temperature counterparts [18]. The behavior of impact diamonds in these essential but yet poorly investigated processes is controlled by their particular origin and properties.

Naturally etched detrital diamonds have pitted or matted (honeycomb) surfaces, rounded edges and corners, and striation in the place of twinning sutures and cracks inherited from graphite crystals. The surface sculptures consisting of numerous intricately shaped steep-walled voids and round or hexagonal pits in the Popigai impact diamonds (Figure 1) are common to other diamonds of this origin. Resorption often produces irregular lacework-looking grains [17,18,25–28].

Surfaces of the Popigai impact diamonds [19,29] are decorated by negatively and positively oriented triangular or hexagonal etch pits, often with irregular contours and rounded corners. These features are similar to those on {111} faces of kimberlitic diamonds because the (0001) plane of graphite is parallel to the (111) plane of cubic diamond.

Impact diamonds often enclose lonsdaleite and both primary and secondary graphite. Lonsdaleite coexists with graphite mainly in grey to black colored diamonds and may constitute up to tens of percent, but it has never been found as a single phase [18,30–32].

On the one hand, polymorphic diamond-to-graphite conversion occurs at >1900 °C and is as fast as 1 min at 1960 °C as shown by experiments with the Popigai impact diamonds, simulating volumetric graphitization in helium, at ambient pressure of 0.1 MPa [33]. On the other hand, the newly formed diamond exposed to impact loading in high-pressure experiments [34] converted back to graphite and became amorphous. The Popigai tagamites are rich in graphite (100/1 relative to diamond), which appears to be mainly residual, i.e., not converted into diamond during the impact event [35], though some diamonds bear signatures of surface graphitization [27,30,36,37].

Unlike diamonds from kimberlites and metamorphic rocks, the impact diamonds remained after their formation in silicate melt at high temperatures ranging from 430 °C to 1730 °C [38], but at a pressure that decreased to nearly ambient after rapid unloading of the target rocks. Presumably significant effects of dissolution or surface graphitization on the diamond potential of rocks in impact craters have never been constrained [17,25]. These processes can be understood by means of etching experiments on kimberlitic diamonds which can highlight various features of grain morphology. We have performed high-temperature ambient-pressure etching experiments in the presence of silicate melt in order to assess the possible postimpact effects on diamond potential in impact craters. While based mainly on our own research, the reported results provide an overview of the available data from the literature as well.

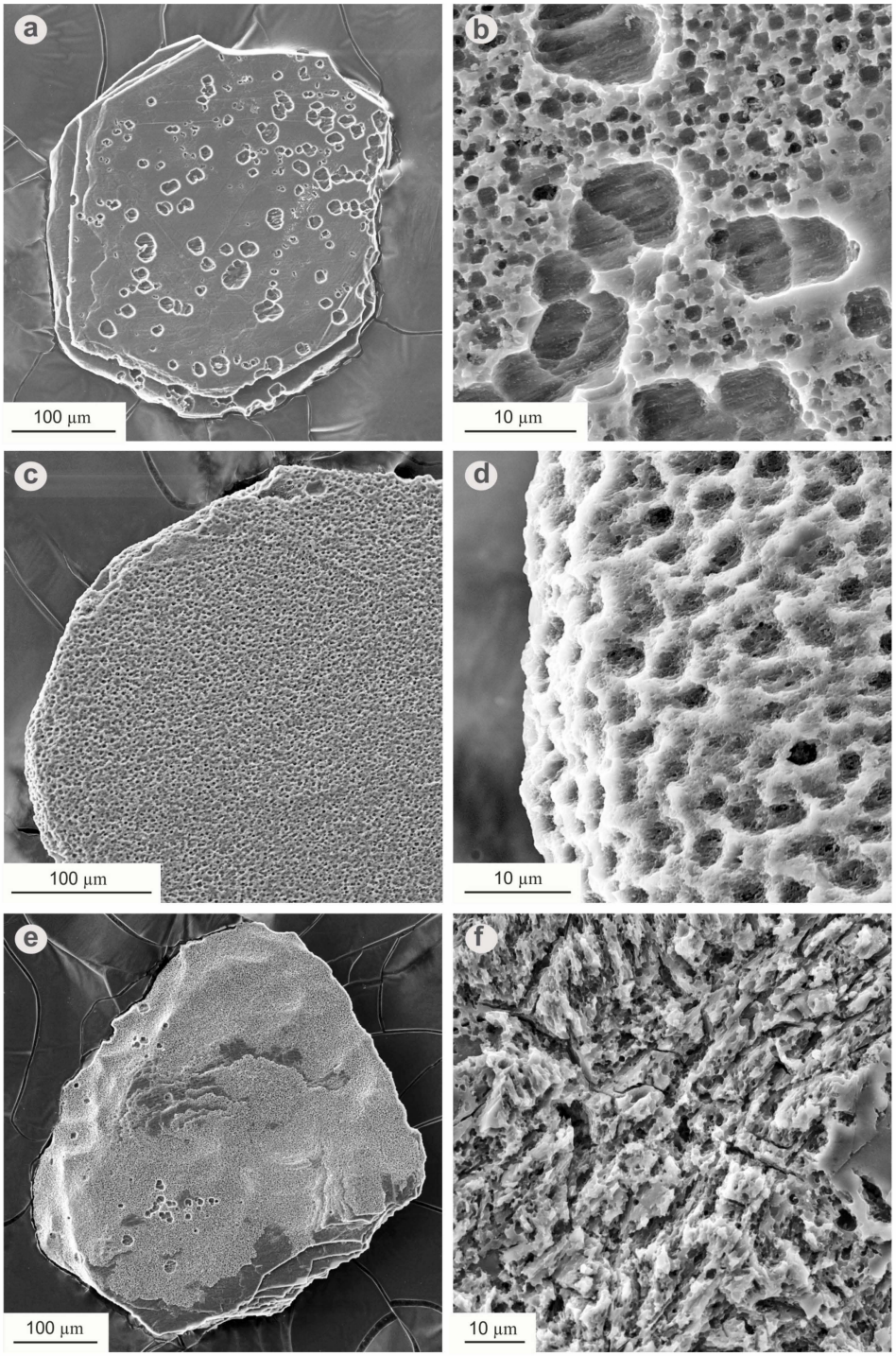

Figure 1. Pitted-honeycomb surfaces of the Popigai impact diamonds.

2. Materials and Methods

The experiments were run at ambient pressure using a vertically positioned tube furnace equipped with a gas conduit that operates in a gas flux mode designed at the V.S. Sobolev Institute of Geology and Mineralogy SB RAS. Quenched glass of natural alkali basalt was used as a silicate melt: 47.0 wt% SiO_2, 2.20 wt% TiO_2, 16.30 wt% Al_2O_3, 3.89 wt% Fe_2O_3, 8.12 wt% FeO, 0.15 wt% MnO, 6.40 wt% CaO, 4.55 wt% MgO, 5.69 wt% Na_2O, 5.0 wt% K_2O, with a total of 99.82 at 0.54 wt% LOI. Basaltic melt is an advantageous etchant due to its relatively low melting point (1080 °C), low viscosity, and high reactivity. Most of the experimental work was carried out at 1130 °C. Capsules with

200 mg ± 10 mg specimens were heated either (1) in the furnace and then quenched to glass or (2) in an environment of inert gas (He or Ar) supplied via a quartz tube or exposed to air. The inert gas was used to control an oxygen partial pressure [39,40] at the hematite–magnetite (HM, Fe_2O_3–Fe_3O_4), nickel-nickel oxide (NNO, Ni–NiO), or carbon-carbon oxide (CCO) buffers. The initial volumetric proportions of components in the buffer mixtures were hematite-magnetite = 4:1 for HM buffer and nickel–nickel oxide = 1:1 for NNO buffer. During a run, the device was in the flow of an inert gas. It is commonly assumed that the buffer technique works and the oxygen fugacity is maintained at a certain level as long as the components of the buffer mixture are retained. The retention of components in buffer mixtures after runs was controlled by XRD analysis. Equilibrium at the level of the CCO buffer was achieved using graphite capsules, closed but not sealed.

The samples were placed in Pt, Mo, Au, or graphite capsules (6 mm inner diameter) depending on the buffer. Then the sample capsules and HM and NNO buffer mixtures were placed in an alundum container with a lid. Separate series of experiments were performed with synthetic matter: Na_2O (20 wt%)–B_2O_3 (40 wt%)–SiO_2 (40 wt%) and Na_2O (30 wt%)–SiO_2 (70 wt%). The procedure was described in detail in earlier publications [41–44].

The experiments dealt with octahedral diamond crystals and 0.6/0.8 mm size powder selected from kimberlite deposits of Sakha Republic (Yakutia). Octahedral crystals had smooth faces without any surface figures or etching sculptures. The edges of crystals had a parallel striation that formed microfacets of rhombodecahedron. Figure 2 shows the examples of the initial diamond surfaces before experimental procedures. The diamond crystals were examined under optical microscopes (MBS-10 and MBI-15). Microphotographs were made using a scanning electron microscope (JSM-35 and TESCAN MIRA 3 LMU, Orsay Holding) in a secondary-electron mode according to the standard procedure at the Analytical Center of the V.S. Sobolev Institute of Geology and Mineralogy (Novosibirsk).

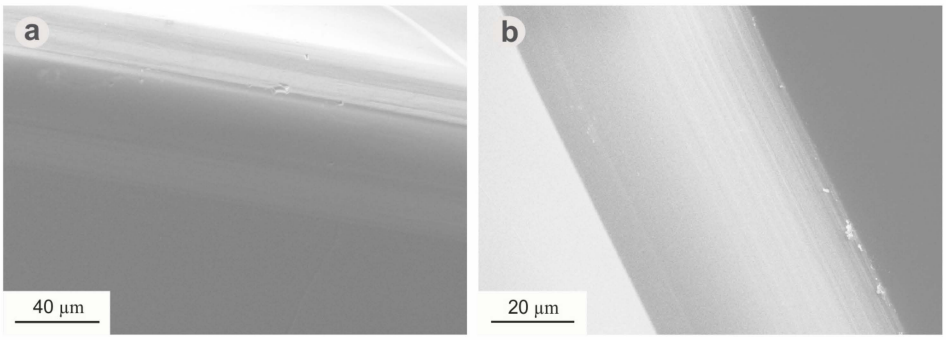

Figure 2. The examples of initial diamond crystal surfaces. Note the absence of any etching sculptures (**a**), except for a slight striation at the edges ((**b**), enlarged view).

3. Results

Oxidation of single-crystal octahedral diamonds in air, without silicate melt, at 1130 °C produced numerous triangular pits of different sizes parallel to {111} faces (Figure 3a–c) as well as positive trigons and surfaces of trisoctahedron (trigon-trioctahedron) with a rough striation near edges of octahedral faces. The morphology evolution of diamonds exposed to oxidation in air was demonstrated in many etching experiments [45–50]. Etching of octahedral diamonds finally leads to the formation of trisoctahedron morphology, but it is rarely observed among natural diamonds [51,52].

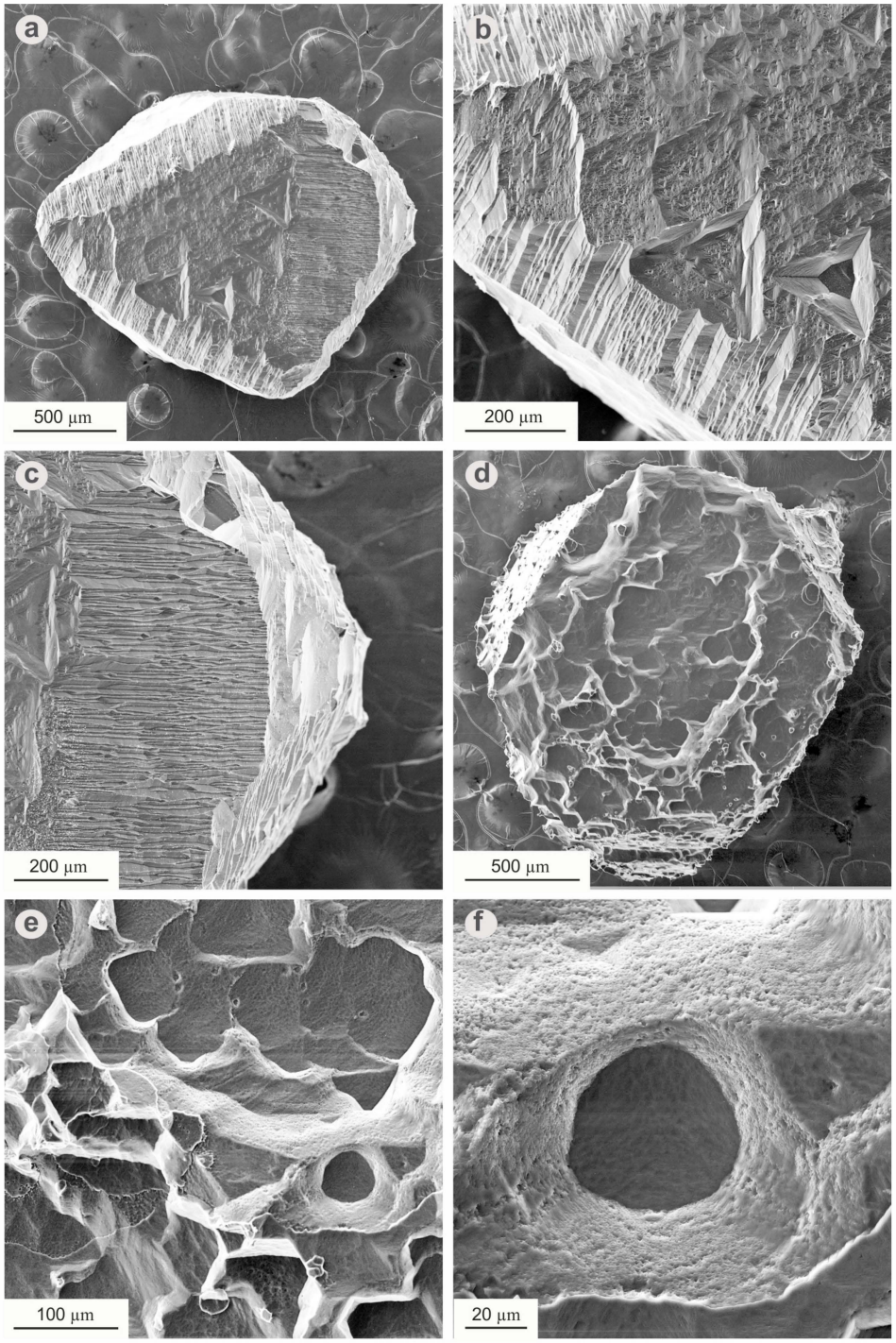

Figure 3. Diamond crystals etched at 1130 °C in air for 15 min (**a**–**c**) and in a basaltic melt exposed to air for 60 min (**d**–**f**). (**a**): general view; (**b**): fragment of an octahedral face with trigons; (**c**): fragment of a crystal with newly formed trisoctahedroidal surfaces; (**d**): general view; (**e**): fragment of an octahedral face with trigonal and hexagonal pits; (**f**): a hexagonal (nearly round) pit on an octahedral face.

The reactions in the presence of B_2O_3-bearing kimberlite melt and air yielded positive trigons on octahedral faces which were further replaced by the rounded trisoctahedron forms [53,54].

The experiment with the basaltic melt–air etchant runs slow since the silicate melt envelops the diamond, the oxidation of which is maintained by oxygen diffusion in the melt [42]. The surface features evolved in several stages under these conditions. Firstly,

flat-bottomed positive trigons appeared on octahedral faces with local trisoctahedroidal surfaces near the edges. Additionally, selective etching produced deep steep-walled hexagonal pits, almost round in shape, or less often triangular pits with truncated vertices. As the etching progressed, the pits coalesced into irregular negative trigons, and the process eventually led to the formation of intricately sculptured crystals with pitted surfaces. As an example, diamond crystal etched at 1130 °C for 60 min lost 25.6% of its original weight (Figure 3d–f). The 0.6/0.8 mm diamond grains subjected to a strong dissolution at the end looked like a "lacework" and had a very large specific surface area [42].

Etching in the basaltic melt at partial oxygen pressure (Po_2) corresponding to HM and NNO buffers [44] caused dramatic changes to the diamond morphology. It was perpendicular to the surface, without formation of layer-by-layer tangential sculpture elements, and without a selective etching. The diamond crystals decreased in size along the contours and retained their octahedral habits (Figure 4) and original surface sculptures, as in the case of a crystal etched under an NNO buffer, which retained its growth steps but acquired rounded contours (Figure 4e).

The process began with negative trigons forming on octahedral diamond faces, more rapidly under the HM buffer, followed by surface graphitization. This phenomenon is common to the evolution of diamond morphology upon etching in basaltic melt under the HM and NNO buffers. The formation of negative trigons, with subsequent graphitization, was observed in other systems, including those without silicate melts [46,55–57], and must be a universal effect. After the crystal surfaces were cleaned to remove graphite, they were found to be covered with numerous irregularly shaped micron-size etching pits and looked matted. That was the case of the crystal in Figure 4d–f which lost 12.3 wt% after 2.5 h etching under the NNO buffer. In the HM buffer conditions, the negative trigons retained their contours but became less regular (e.g., the crystal in Figure 4a–c lost 17.4 wt% after 3.5 h of HM buffering).

Diamond etching in the basaltic melt under the CCO buffer led to a surface graphitization that occurred in the same way as in the case of HM and NNO buffers [41]. After the removal of graphite, the diamonds in these runs likewise had matted surfaces with numerous irregularly shaped small pits (e.g., the crystal in Figure 5a,b lost 11.65% of its original weight after 14 h of etching at 1200 °C). However, the crystal faces bore signatures of interaction with drops of iron melt which can form under the reduced CCO conditions at a normal total pressure [58]. At temperatures below the melting point of basalt, iron reduction occurred as well. The iron particles produced irregular pits on the diamond surface, but the etching process ground to a halt due to low carbon solubility in iron. The diamond crystal in Figure 5c,d lost only 0.4 wt% after 120 h of etching at 1000 °C.

Our results on diamond etching in reduced conditions under the CCO buffer are consistent with the published evidence. For instance, graphitization was observed on octahedral diamonds etched in a kimberlite melt (1450 °C) in a nitrogen flux using an open graphite capsule [59]. Kimberlite melting (1200 °C) was accompanied by melt ebullition and flotation of diamond crystals. The sculptures on their {111} faces differed depending on whether they interacted with gas or melt: negative trigons with some graphite films (gas contact) or strong resorption and irregular etching features not related to the facet crystallography (melt contact). Irregularly shaped pits, graphite films, and metallic iron on diamond surfaces were also reported [60] for natural octahedral and dodecahedral diamonds exposed to etching in kimberlite melt in vacuum (~0.133 Pa) at 1600 °C.

In experiments at 1100 °C (60 min run), diamond obviously did not interact with a synthetic iron-free Na_2O–B_2O_3–SiO_2 silicate melt in argon and hydrogen fluxes: it neither exhibited a change in the micromorphology of faces nor lost its weight. However, oxidation occurred in Na_2O–SiO_2 and Na_2O–B_2O_3–SiO_2 silicate melts in air [61], though the reaction with the Na_2O–SiO_2 melt was very slow with minor weight loss at a rate close to the rate of surface graphitization under the CCO buffer conditions [41].

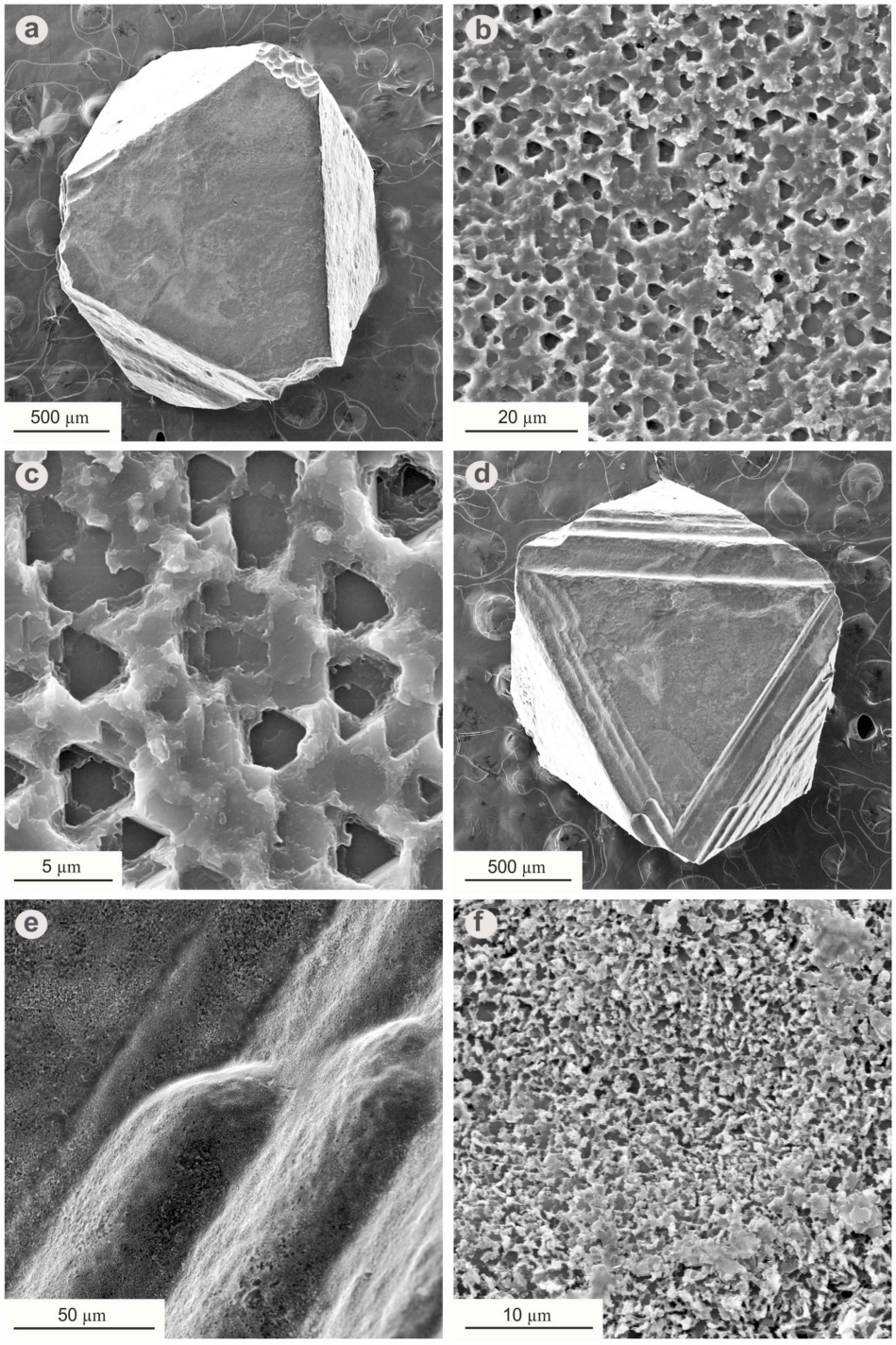

Figure 4. Diamond crystals etched at 1130 °C in a basaltic melt, under the HM buffer, for 3.5 h (**a**–**c**) and under the NNO buffer for 2.5 h (**d**–**f**). (**a**): general view; (**b**,**c**): fragments of an octahedral face with trigonal, truncated trigonal, and hexagonal pits; (**d**): general view; (**e**): preserved growth steps; (**f**): dissolution sculptures on an octahedral face resulting from surface graphitization.

Octahedral diamonds etched in a Na_2O–SiO_2 melt developed unevenly matted surfaces with etching features not related to facet crystallography and randomly oriented irregular pits or, locally, with micron-size negative trigons. The interaction with a Na_2O–B_2O_3–SiO_2 melt produced 20 μm to 260 μm disc-shaped sculptures with tiny irregular pits, as well as small negative trigons. The mixed (1:1 in weight) synthetic Na_2O–B_2O_3–SiO_2 glass + basalt etchant caused the formation of positive trigons on the {111} faces.

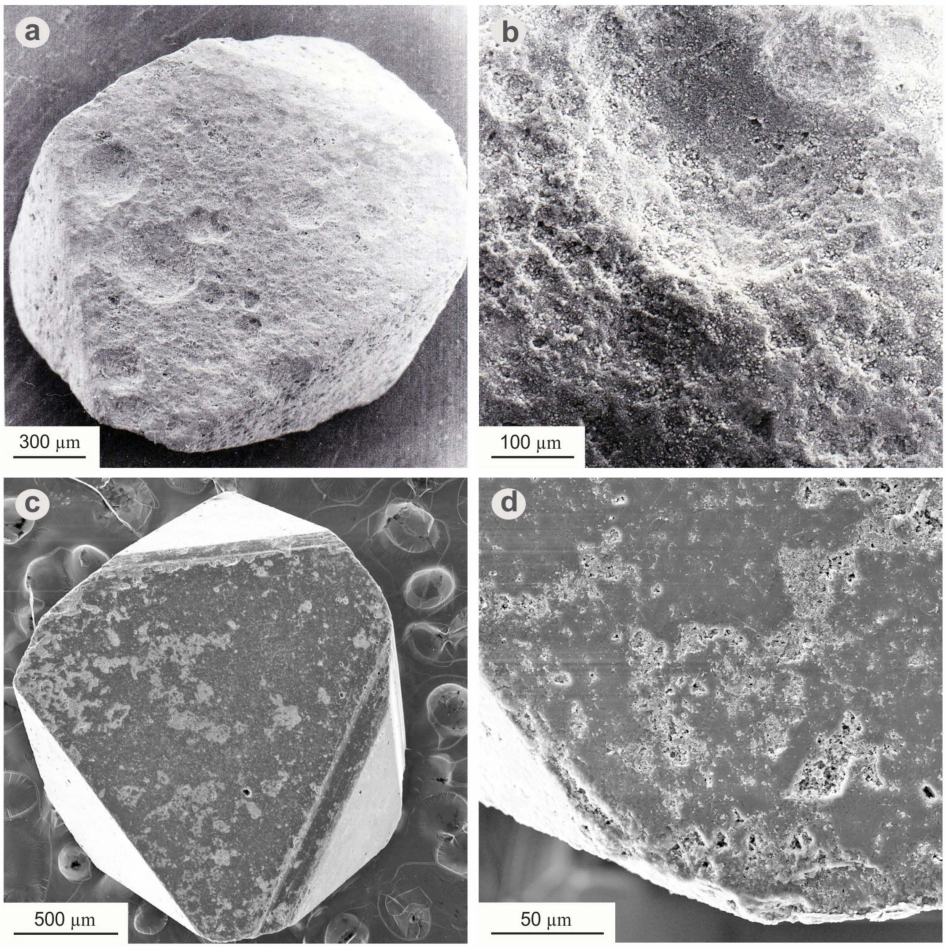

Figure 5. Diamond crystals etched in the presence of a basaltic melt, under the CCO buffer, at 1200 °C for 14 h (**a**,**b**) and at 1000 °C for 120 h (**c**,**d**). (**a**,**c**): general view; (**b**,**d**): fragments of an octahedral face with etching sculptures resulting from surface graphitization and round pits produced by interaction with solid iron particles.

The etching rates were determined as 0.004, 0.01, and 0.017 mg/h for Na_2O–SiO_2, Na_2O–B_2O_3–SiO_2, and Na_2O–B_2O_3–SiO_2 + basalt melts, respectively. Although the difference was quite moderate, there were considerable surface changes due to the rate of oxygen diffusion in the melts of different viscosity which depends on their SiO_2 content [61]. The ambient conditions being the same, the etching rates were always higher for the 0.6/0.8 mm diamonds than for the octahedral varieties (Figure 6) because the former lacked singularity and had less specific surface area. The etching patterns obtained in the experiments are summarized in Table 1.

Table 1. Surface sculptures on {111} faces of diamonds etched in silicate melts at 0.1 MPa.

Etchant	T, °C	Etching Sculptures
Na_2O–B_2O_3–SiO_2, Ar	1100	None
Na_2O–B_2O_3–SiO_2, H_2	1100	None
Na_2O–B_2O_3–SiO_2, air	1000	Discoids, negative trigons
Na_2O–SiO_2, air	1000	Irregular etch pits and negative trigons (matted surfaces)
Na_2O–B_2O_3–SiO_2 and basalt (1:1), air	1000	Positive trigons, hexagonal etch pits
Basalt, air	1130	Positive trigons, hexagonal etch pits
Basalt, HM buffer	1130	Negative trigons, often with canted corners
Basalt, NNO buffer	1130	Negative trigons, irregular etch pits
Basalt, CCO buffer	1200	Round pits with a spherical bottom; corrosion textures with irregular nonaligned etch pits

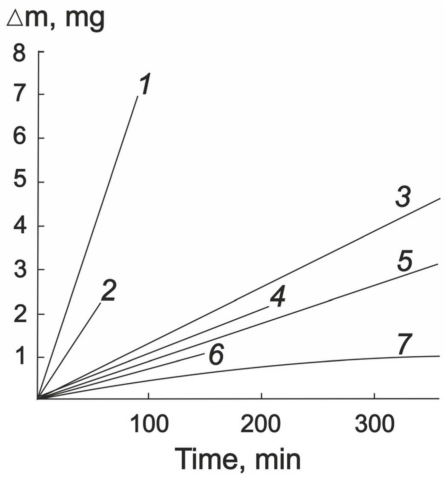

Figure 6. Weight loss (Δm) as a function of run duration of diamonds etched in a basalt melt at 1130 °C and at different fO_2: 1, 3, 5 = diamonds of fraction 0.6/0.8 mm exposed to air, under HM and NNO buffers, respectively; 2, 4, 6, 7 = octahedral diamonds exposed to air, under the HM, NNO, and CCO buffers, 1200 °C, respectively, complementing [44].

4. Discussion

The reported experiments on diamond etching in silicate melts at ambient pressure have a number of important implications. Iron-free silicate melts do not interact with diamond in the presence of an inert gas, but the reaction occurs in air on account of oxygen, which is a strong oxidizer of carbon and, hence, diamond. The oxidation rate is slower with silicate melt than without it, as it protects the diamond surfaces from O_2.

Diamond oxidation under the HM, NNO, and CCO buffer conditions is made possible by oxygen diffused into silicate melt from the gaseous environment. The diffusion rate is inversely proportional to the melt viscosity [62,63], and the depth of interaction and the morphology of diamond crystals depend on the melt composition. At the same time, the experiments with melts of the same composition but at different oxygen partial pressures demonstrated that the etching rates and etching figures are sensitive to the environment composition. Etching in the range from strongly oxidized to reduced conditions produced the diversity of surface figures which are obviously controlled by oxygen partial pressure: positive trigons at high Po_2; hexagonal pits at intermediate conditions; and negative trigons or irregular dissolution sculptures, graphite films, and round pits made by iron melt drops at low Po_2.

Etching in a gaseous environment at the NNO buffer produced positive trigons with obtuse corners at 1000 °C [43], mainly hexagonal features at 1100 °C, and negative trigons at 1200 °C; graphite appeared locally on diamond surfaces in the 1100–1200 °C temperature interval. Under the HM buffer conditions, the positive trigons with obtuse corners formed at 1100 °C, while hexagonal pits and negative trigons appeared at 1200 °C. Under ambient pressure, the inversion of etching pits on {111} faces occurred gradually, at least within a 150 °C range at the same Po_2.

The highly reduced conditions corresponding to CCO equilibrium (Figure 7) are sufficient for the formation of metallic iron (iron–wüstite (IW) and iron–quartz–fayalite (IQF) buffers) and surface graphitization [64]. At the temperatures and pressures corresponding to the stability of graphite, the Po_2 is lower in equilibrium with diamond than with graphite. The oxidized carbon species equilibrated with diamond reach higher concentrations since diamond is unstable and becomes oxidized in these conditions, while graphite forms from carbon supersaturated fluid.

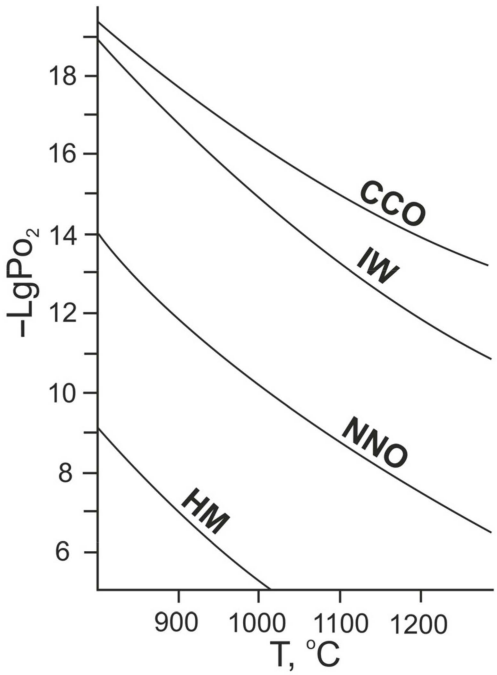

Figure 7. Equilibrium oxygen partial pressure for buffer reactions at 0.1 MPa (after [64]).

The grain morphology of natural impact diamonds may evolve in different redox environments. Two opposite scenarios are possible in the presence of carbon: either Po_2 is controlled externally, e.g., by diffusion of oxygen, or the system reaches the CCO equilibrium on account of the carbon (graphite or diamond) it contains [58]. Therefore, the etching figures produced by the silicate melt depend on the etching rate, which is in turn controlled by Po_2 and air access as in the case of impact diamond. The distance between diamond crystal and the air contact depends upon the volume of molten rock, as shown in Figure 8. The crystals near the contact are expected to develop mostly hexagonal pits, while those located deeper within the molten rock have graphite films and irregular randomly oriented etching sculptures on their surfaces.

Impact diamonds most often show pitted-honeycomb surfaces with hexagonal to nearly rounded etching pits [17,18,25,28,29,65]. Numerous pits of similar sizes (as in Figure 1) are the result of a very fast etching perpendicular to the surface known as a "normal type of etching" [66]. Therefore, the oxidation of diamonds in a cooling impact melt was a quite rapid event that caused a small effect only. For instance, a 0.7 mm diamond became fully oxidized by air oxygen during 2.5 h at 1000 °C [43]. In the other extreme case, with CCO-buffered Po_2, the surface graphitization can eliminate the diamond in ~3 years. Although silicate melts protect diamonds from oxidation, natural melts are hotter than the experimental 1130 °C etchants which can oxidize a 7 mg 0.6/0.8 mm specimen in less than 20 min in air [42] and in 90 min in basaltic melt + air medium (Figure 6).

The basalt we used in our experiments contained less SiO_2 than the Popigai graphite-bearing gneisses and tagamites; thus, its melt was less viscous. The etching rate of diamond from the Popigai tagamites estimated with reference to the data for 1130 °C viscous synthetic melts is 0.2–0.3 mg/h. Furthermore, the hard crust that appeared during the melt quenching should interrupt the oxygen diffusion, thus protecting diamonds from etching with only residual etching effects present. As a result, the highest diamond contents are identified in the unmolten impact metamorphic gneisses, the relative average contents in tagamites and zuvites being at the ratio of 3:2 [18].

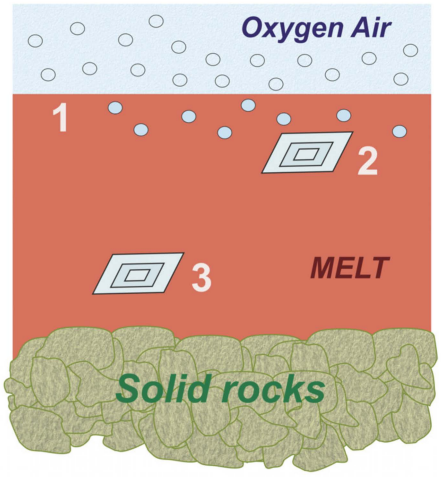

Figure 8. Schematic drawing of the possible positions of diamond crystals in molten rocks of an impact crater: (1)—surface of melt; (2)—crystal near the surface: mainly hexagonal or round pits; (3)—crystal deep within molten rock: irregular randomly oriented pits produced by surface graphitization.

The oxidation and surface graphitization can also result from the effect of water [67], which is a strong oxidizer at temperatures over 1000 °C [68]. High H_2O content in gneisses of the Popigai impact crater was determined during its early studies [69,70]. The Popigai tagamites contain either 2.23 ± 0.48 wt% or 0.74 ± 0.18 wt% H_2O, while the dry varieties show a 30–40% higher diamond enrichment compared with the wet rocks [18,71].

5. Conclusions

The reported results allow the following inferences:

1. Diamond crystals inevitably experience natural oxidation and surface graphitization during pressure decrease at high residual temperatures within the molten target rocks after an impact event.
2. Natural etching of diamonds in silicate melt can occur in a wide range of oxidation conditions controlled by O_2 diffusion.
3. Some impact diamonds located near the surface of the molten rock were oxidized at the highest rates.
4. The preservation of diamonds deep within the melt was possible due to protection from oxidizing agents.

The surface features obtained in the reported etching experiments on common diamonds are similar to those of natural impact diamonds, with some difference in macromorphology due to the origin of impact diamonds by martensitic transformation of graphite.

Author Contributions: Conceptualization, writing—original draft preparation, V.S., V.A.; resources, A.C. (Anatoly Chepurov); funding acquisition, project administration, N.P.; methodology, E.Z.; investigation, A.C. (Aleksei Chepurov), I.G. All authors have read and agreed to the published version of the manuscript.

Funding: This research was funded by the Ministry of Science and Higher Education of the Russian Federation grant No. 075-15-2020-781.

Acknowledgments: The authors thank two anonymous reviewers for the comprehensive reviewing of the manuscript.

Conflicts of Interest: The authors declare no conflict of interest.

References

1. Arima, M. Experimental study of growth and resorption of diamond in kimberlitic melts at high pressure and temperatures. In Proceedings of the 3rd NIRIM International Symposium on Advanced Materials (ISAM'96), Tsukuba, Japan, 4–8 March 1996; pp. 223–228.
2. Sonin, V.M.; Zhimulev, E.I.; Chepurov, A.I.; Afanasiev, V.P. Morphology of diamond crystals etched in a kimberlite melt at high PT parameters. *Izvestiya Vysshykh Uchebnykh Zavedeniy Geologiya Razvedka* **2002**, *1*, 60–69. (In Russian)
3. Sonin, V.M.; Zhimulev, E.I.; Tomilenko, A.A.; Chepurov, S.A.; Chepurov, A.I. Chromatographic study of diamond etching in kimberlitic melts in the context of diamond natural stability. *Geol. Ore Deposit.* **2004**, *46*, 182–190.
4. Kozai, Y.; Arima, M. Experimental study on diamond dissolution in kimberlitic and lamproitic melts at 1300–1420 °C and 1 GPa with controlled oxygen partial pressure. *Am. Mineral.* **2005**, *90*, 1759–1766.
5. Fedortchouk, Y.; Canil, D.; Semenets, E. Mechanism of diamond oxidation and their bearing on the fluid composition in kimberlitic magmas. *Am. Mineral.* **2007**, *92*, 1200–1212.
6. Khokhryakov, A.F.; Pal'yanov, Y.N. The evolution of diamond morphology in the process of dissolution: Experimental data. *Am. Mineral.* **2007**, *92*, 909–917. [CrossRef]
7. Arima, M.; Kozai, Y. Diamond dissolution rates in kimberlitic melts at 1300–1500 °C in the graphite stability field. *Eur. J. Mineral.* **2008**, *20*, 357–364. [CrossRef]
8. Fedortchouk, Y. A new approach to understanding diamond surface features based on a review of experimental and natural diamond studies. *Earth Sci. Rev.* **2019**, *193*, 45–65. [CrossRef]
9. Chepurov, A.I.; Sonin, V.M.; Zhimulev, E.I.; Chepurov, A.A.; Pomazansky, B.S.; Zemnukhov, A.L. Dissolution of diamond crystals in a heterogeneous (metal–sulfide–silicate) medium at 4 GPa and 1400 °C. *J. Mineral. Petrol. Sci.* **2018**, *113*, 59–67. [CrossRef]
10. Chepurov, A.I.; Sonin, V.M.; Zhimulev, E.I.; Chepurov, A.A. Preservation conditions of CLIPPIR diamonds in the earth's mantle in a heterogeneous metal–sulphide–silicate medium (experimental modeling). *J. Mineral. Petrol. Sci.* **2020**, *115*, 236–246. [CrossRef]
11. Sonin, V.M.; Zhimulev, E.I.; Pomazanskiy, B.S.; Zemnuhov, A.L.; Chepurov, A.A.; Afanasiev, V.P.; Chepurov, A.I. Morphological features of diamond crystals dissolved in $Fe_{0.7}S_{0.3}$ melt at 4 GPa and 1400 °C. *Geol. Ore Deposit.* **2018**, *60*, 82–92. [CrossRef]
12. Sonin, V.M.; Zhimulev, E.I.; Chepurov, A.A.; Lindenblot, E.S.; Logvinova, A.M.; Shcheglov, D.V.; Pomazanskii, B.S.; Afanas′ev, V.P.; Chepurov, A.I. Dissolution of natural octahedral diamonds in an Fe–S melt at high pressure. *Geol. Ore Deposit.* **2020**, *62*, 497–507. [CrossRef]
13. Gryaznov, I.A.; Zhimulev, E.I.; Sonin, V.M.; Lindenblot, E.S.; Chepurov, A.A.; Sobolev, N.V. Morphological features of diamond crystals resulting from dissolution in a Fe–Ni–S melt under high pressure. *Dokl. Earth Sci.* **2019**, *489*, 1449–1452. [CrossRef]
14. Smith, E.M.; Shirey, S.B.; Nestola, F.; Bullock, E.S.; Wang, J.; Richardson, S.H.; Wang, W. Large gem diamonds from metallic liquid in Earth's deep mantle. *Science* **2016**, *35*, 1403–1405. [CrossRef]
15. Smith, E.M.; Shirey, S.D.; Wang, W. The very deep origin of the World's biggest diamond. *Gems Gemol.* **2017**, *53*, 388–403. [CrossRef]
16. Grieve, R.A.F. Economic natural resource deposits at terrestrial impact structures. Mineral Deposits and Earth Evolutions. *Geol. Soc. Spec. Publ.* **2005**, *248*, 1–29.
17. Vishnevsky, S.A.; Afanasiev, V.P.; Argunov, K.P.; Palchik, N.A. *Impact Diamonds: Their Features, Origin and Significance*; SB RAS, UIGGM: Novosibirsk, Russia, 1997; 53p. (In Russian)
18. Masaitis, V.L.; Mashchak, M.S.; Raichlin, A.I.; Selivanovskaya, T.V.; Shafranovsky, G.I. *Diamond-Bearing Impactites of the Popigai Astrobleme*; VSEGEI: Saint Petersburg, Russia, 1998; 179p. (In Russian)
19. Kvasnytsya, V.N.; Zintchouk, N.N.; Koptil, V.I. *Typomorfism of Diamond Microcrystals*; Nedra Business Center: Moscow, Russia, 1999; 224p. (In Russian)
20. Masaitis, V.L. Impact diamonds of the Popigai Astrobleme: Main properties and practical use. *Geol. Ore Deposit.* **2013**, *55*, 607–612. [CrossRef]
21. Pokhilenko, N.P. Mineral budget of the republic of Sakha (Yakutia) Arctic Zone. *Econ. Russ. East* **2015**, *2*, 12–20. (In Russian)
22. Shafranovsky, G.I. Crystallomorphology of diamonds on graphite. *Zap. Vsesoyuznogo Mineral. Obs.* **1985**, *114*, 30–34. (In Russian)
23. Erskine, D.J.; Nellis, W.J. Shock-induced martensitic phase transformation of oriented graphite to diamond. *Nature* **1991**, *349*, 317–319. [CrossRef]
24. Kurdyumov, A.V.; Britun, V.F.; Yarosh, V.V.; Danilenko, A.I.; Zelyavskii, V.B. The influence of the shock compression conditions on the graphite transformations into lonsdaleite and diamond. *J. Superhard. Mater.* **2012**, *34*, 19–27. [CrossRef]
25. Valter, A.A.; Yeremenko, G.K.; Kvasnytsya, V.N.; Polkanov, Y.A. *Shock-Metamorphic Minerals of Carbon*; Nauk. Dumka: Kiev, Ukraine, 1992; 170p. (In Russian)
26. Kaminsky, F.V.; Blinova, T.K.; Galimov, E.M.; Klyuev, Y.A.; Kodina, L.A.; Koptil', V.I.; Krivonos, V.S.; Frolova, L.N.; Khrenov, A.Y. Polycrystalline aggregates of diamond with lonsdaleite from placers of Yakutia. *Mineral. J.* **1985**, *7*, 27–35. (In Russian)
27. Masaitis, V.L.; Shafranovsky, G.I.; Grieve, R.; Perederi, U.V.; Balmasov, E.L.; Fedorova, I.G. Diamonds from suevite in the Sudbury impact structure, Ontario, Canada. *Zap. Rossiiskogo Mineral. Obs.* **1997**, *126*, 1–6. (In Russian)
28. Pratesi, G.; Guidice, A.L.; Vishnevsky, S.; Manfredotti, C.; Cipriani, C. Cathodoluminescence investigation on the Popigai, Ries, and Lappajärvi impact diamonds. *Am. Mineral.* **2003**, *88*, 1778–1787.
29. Kvasnytsya, V.; Wirth, R.; Piazolo, S.; Jacob, D.T.; Trimby, P. Surface morphology and structural types of natural impact apographitic diamonds. *J. Superhard Mater.* **2016**, *38*, 71–84. [CrossRef]

30. Valter, A.A.; Kvasnytsya, V.N.; Yeremenko, G.K. Structure, composition, and optical properties of diamond paramorphs after graphite. *Mineral. J.* **1990**, *12*, 3–16. (In Russian)
31. Ohfuji, H.; Irifune, T.; Litasov, K.D.; Yamashita, T.; Isobe, F.; Afanasiev, V.P.; Pokhilenko, N.P. Natural occurrence of pure nano-polycrystalline diamond from impact crater. *Sci. Rep.* **2015**, *5*, 14702. [CrossRef] [PubMed]
32. Yelisseyev, A.; Gromilov, S.; Afanasiev, V.; Sildos, I.; Kiisk, V. Effect of lonsdaleite on the optical properties of impact diamonds. *Diam. Rel. Mater.* **2020**, *101*, 107640. [CrossRef]
33. Gromilov, S.A.; Nikolaev, R.E.; Cherepanova, S.V. Formation of compressed and mixed-layer graphite upon heating impact diamonds. *J. Struct. Chem.* **2018**, *59*, 355–364. [CrossRef]
34. Kenkmann, T.; Hornemann, U.; Stöffler, D. Experimental shock synthesis of diamonds in a graphite gneiss. *Meteorit. Planet. Sci.* **2005**, *40*, 1299–1310. [CrossRef]
35. Afanasiev, V.; Gromilov, S.; Sonin, V.; Zhimulev, E.; Chepurov, A. Graphite in rocks of the Popigai impact crater: Residual or retrograde? *Turk. J. Earth Sci.* **2019**, *28*, 470–477. [CrossRef]
36. Masaitis, V.L.; Shafranovsky, G.I.; Fedorova, I.G. The apographitic impact diamonds from astroblemes Ries and Popigai. *Zap. Rossiiskogo Mineral. Obs.* **1995**, *124*, 12–19. (In Russian)
37. Valter, A.A.; Yeremenko, G.K.; Polkanov, Y.A.; Siebenschock, M.; Schmitt, R.T.; Stöffler, D. Impact diamond from zuvites of the Ries crater (Germany): New data. *Mineral. J.* **1998**, *20*, 3–12. (In Russian)
38. Vishnevsky, S.A. *Astroblemes*; Nonparel: Novosibirsk, Russia, 2007; 288p. (In Russian)
39. Huebner, J.S. Buffering techniques for hydrostatic systems at elevated pressures. In *Research Techniques for High Pressures and Temperatures*; Ulmer, G.C., Ed.; Springer: Berlin/Heidelberg, Germany, 1971; pp. 123–177.
40. Gramenitsky, E.N.; Kotel′nikov, A.R. *Experimental Petrography*; Moscow University Press: Moscow, Russia, 1984; 252p. (In Russian)
41. Sonin, V.M.; Afanas′ev, V.P.; Chepurov, A.I. Stability of diamond under reducing conditions (at the level of the CCO buffer) in the presence of silicate melt. In *Materials on Genetic and Experimental Mineralogy*; SB RAS: Novosibirsk, Russia, 1995; Volume 11, pp. 98–110. (In Russian)
42. Sonin, V.M.; Zhimulev, E.I.; Naberukhina, A.V. Peculiarities of diamond etching in basalt melt at atmospheric pressure. *Izvestiya Vysshykh Uchebnykh Zavedeniy Geologiya Razvedka* **2000**, *1*, 60–69. (In Russian)
43. Sonin, V.M.; Fedorov, I.I.; Pokhilenko, L.N.; Pokhilenko, N.P. Diamond oxidation rate as related to oxygen fugacity. *Geol. Ore Deposit.* **2000**, *42*, 496–502.
44. Sonin, V.M.; Zhimulev, E.I.; Fedorov, I.I.; Chepurov, A.I. Effect of oxygen fugacity on etching rate of diamond crystals in silicate melt. *Geol. Ore Deposit.* **2006**, *48*, 499–501. [CrossRef]
45. Kukharenko, A.A.; Titova, V.M. New data on the solution of diamond crystals. *Uch. Zap. Leningr. Gos. Univ. Ser. Geol. Nauk.* **1957**, *215*, 108–134. (In Russian)
46. Evans, T.; Sauter, D.H. Etching of diamond surfaces with gases. *Phil. Mag.* **1961**, *6*, 429–440.
47. Patel, A.R.; Agarwal, M.K. Fast etching of diamond surfaces. *Surf. Sci.* **1965**, *3*, 502–505.
48. Patel, A.R.; Agarwal, M.K. Studies of etch rates of different faces on natural diamond. *Ind. Diamond Rev.* **1966**, *26*, 334–336.
49. Varshavsky, A.V. Thermal etching of diamond crystals in air. *Zap. Rossiiskogo Mineral. Obs.* **1965**, *94*, 471–475. (In Russian)
50. Uspenskaya, K.S.; Tolmachev, Y.N.; Fedoseev, D.V. Oxidation and graphitization of diamond at low pressures. *Russ. J. Phys. Chem.* **1982**, *56*, 495–496. (In Russian)
51. Bartoshinsky, Z.V.; Kvasnytsya, V.N. *Crystalomorphology of Diamonds from Kimberlites*; Nauk. Dumka: Kiev, Ukraine, 1991; 172p. (In Russian)
52. Sonin, V.M.; Zhimulev, E.I.; Afanas′ev, V.P.; Chepurov, A.I. Genetic aspects of the diamond morphology. *Geol. Ore Deposit.* **2002**, *44*, 291–299.
53. Nardov, V.M. Crystal photograms etched in a kimberlite melt. *Zap. Rossiiskogo Mineral. Obs.* **1958**, *87*, 612–614. (In Russian)
54. Titova, V.M. New data on the dissolution of diamond. *Zap. Rossiiskogo Mineral. Obs.* **1962**, *91*, 334–337. (In Russian)
55. Seal, M. Graphitization and plastic deformation of diamond. *Nature* **1958**, *182*, 1264–1267. [CrossRef]
56. Howes, V.R. The graphitization of diamond. *Proc. Phys. Soc.* **1962**, *80*, 648–661. [CrossRef]
57. Titova, V.M.; Futergendler, S.I. On orientation of graphite formed on diamond as a result of its allotropic transformation on heating. *Kristallografiya* **1962**, *7*, 925–929. (In Russian)
58. Kadik, A.A.; Lukanin, O.A. *Outgassing of the Upper Mantle Upon Melting*; Nauka: Moscow, Russia, 1986; 97p. (In Russian)
59. Frank, F.C.; Puttic, K.E. Etch pits and trigons on diamond. II. *Phill. Mag.* **1958**, *3*, 1273–1279.
60. Harris, J.W.; Vance, E.R. Studies of the reaction between diamond and kimberlite. *Contrib. Mineral. Petrol.* **1974**, *47*, 237–244.
61. Sonin, V.M.; Naberukhina, A.V.; Fedorova, E.N.; Turkin, A.I. Etching of diamond in a silicate melt at atmospheric pressure. *Zap. Rossiiskogo Mineral. Obs.* **2000**, *129*, 76–81. (In Russian)
62. Epelbaum, M.B. *Silicate Melts with Volatile Components*; Nauka: Moscow, Russia, 1980; 255p. (In Russian)
63. Dunn, T. Oxygen chemical diffusion in three basaltic liquids at elevated temperatures and pressures. *Geochim. Cosmochim. Acta* **1983**, *47*, 1923–1930. [CrossRef]
64. Chepurov, A.I.; Fedorov, I.I.; Sonin, V.M. *Experimental Modelling of the Diamond Formation Processes*; SB RAS, SPC UIGGM: Novosibirsk, Russia, 1997; 196p. (In Russian)
65. Osovetsky, B.M.; Naumova, O.B. The micro- and nanoforms of impact diamonds surface. *Bull. Perm Univ. Geol.* **2014**, *2*, 8–19. (In Russian) [CrossRef]

66. Sangwal, K. *Etching of Crystals: Theory, Experiment, and Application*; Science: Amsterdam, The Netherlands, 1987; 497p.
67. Sonin, V.M.; Gryaznov, I.A.; Chepurov, A.I.; Pokhilenko, N.P. H_2O—As a possible initiator of surface graphitization of impact diamonds. *Dokl. Earth Sci.* **2021**, *498*, 388–391. [CrossRef]
68. Zhdankina, O.Y.; Kulakova, I.I.; Rudenko, A.P. Oxidation of kimberlite diamonds with mixtures of carbon dioxide and water vapor. *Mosc. Univ. Chem. Bull.* **1985**, *26*, 497–501. (In Russian)
69. Masaitis, V.L.; Futergendler, S.I.; Gnevushev, M.A. Diamonds in impactites of the Popigai meteoritic crater. *Zap. Vsesoyuznogo Mineral. Obs.* **1972**, *101*, 108–112. (In Russian)
70. Dolgov, Y.A.; Vishnevsky, S.A.; Shugurova, N.A. Gas inclusions in impactites. In *Thermobarogeochemistry and Genetic Mineralogy*; Dolgov, Y.A., Ed.; IGG SB AS USSR: Novosibirsk, Russia, 1975; pp. 129–140. (In Russian)
71. Vishnevsky, S.A. Water and diamond potential of the Popigai impactites-tagamites. In Proceedings of the Magmatism and Metamorphism in the Earth's History, Book of Abstracts, XIth Petrographic Conference, Yekaterinburg, Russia, 24–28 August 2010; Volume 1, pp. 120–121.